Three fundamental granular flow experiments and CPFD predictions

Dale M. Snider

Arena-flow, LLC, United States

Abstract

Granular flow of three granular flow experiments is predicted by a computational particle fluid dynamic CPFD numerical scheme in three dimension using the true particle size distribution. The experiments are simple which show the characteristics of particle flow which differs from fluid flow. The experiments are flow of particles in sedimentation, a U-tube and from a hopper. The CPFD method models the fluid as a fluid and models the particles as discrete particles (material description). The CPFD method is a form of discrete element method, where each particle has three-dimensional forces from fluid drag, gravity, static–dynamic friction, particle collision and possibly other forces. However, unlike DEM models which calculate particle-to-particle force by a spring–damper model and direct particle contact, the CPFD method models collision force on each particle as a spatial gradient. The CPFD numerical method predictions compare well with all three experiments with no adjustment of parameters or empirical correlations between calculations.
© 2007 Elsevier B.V. All rights reserved.

Keywords: Particle; Granular; DEM; CPFD; Lagrangian; Particle experiments

1. Introduction

The flow of granular material can be considerably different than a fluid. A good example is the hour glass. The hour glass works as a useful measure of time because the particle flow through the orifice is constant. If instead, a fluid were used in the hour glass, the flow rate is initially high because of a hydrostatic head, and the flow tapers off as the hour glass empties of fluid. Presented here are basic granular flows which show the characteristics of particle flow. Many of the examples are not described by a fluid or because of the influence of particle size or density distribution, are not effectively calculated by a pseudo-continuum particle model. The examples are simple which allows the granular behavior to be seen and not lost in complex geometry or boundary conditions.

The granular flow is predicted with a computation particle fluid dynamic (CPFD) numerical method. The numerical method is in the direct element method (DEM) class of solutions. Continuum or fluid models (Eulerian reference frame) readily allow modeling of forces using spatial gradients of properties [1,2]. However, modeling a distribution of types and sizes of particles complicates the continuum formulation

because separate continuity and momentum equations must be solved for each size and type [2,3]. Further the pseudo-continuum approximation may be taxed in modeling solid granular material as a continuum. The Lagrangian or material description for the particle phase (DEM fits into Lagrangian solution methods) allows economical solution for flows with a wide range of particle types, sizes, shapes and velocities [4] and has no numerical diffusion associated with an advection operator. Because of the computational complexity of calculating dense particle–particle interactions, traditional DEM methods have been limited to on the order of 2×10^5 particles and are often restricted to two-dimensional solutions and often without a fluid phase. The calculation method by Snider [5] described here and applied to granular flow problems in this paper uses features from the Eulerian method and features from the material or Lagrangian method. This computational particle fluid dynamic (CPFD) method models the fluid as a fluid and models the particles as discrete particles (material description). The CPFD method is a form of discrete element method, where each particle has three-dimensional forces from fluid drag, gravity, static–dynamic friction, particle collision and possibly other forces. However, unlike DEM models which calculate
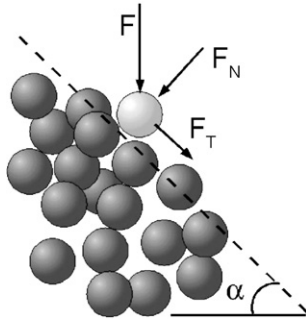
Fig. 1. Particles on an inclined plane and on packed bed.

Fig. 3. CPFD predicted sedimentation rate compared to measured data by Davis et al. [11].

particle-to-particle force by a spring–damper model and direct particle contact, the CPFD method models collision force on each particle as a spatial gradient. A CPFD particle, in dense particle flow, knows it will hit another particle(s) but it does not care which other particle(s) it hits. Similar for all other particles. O'Rourke and Amsden [6] introduced the concept of applying spatial gradients to discrete particles in chemically reacting flow. O'Rourke later extended the idea to calculating the particle normal stress from a spatial gradient [7], and Snider et al. [8] applied a two-dimensional discrete particles method to sedimentation using an implicit particle normal stress as a
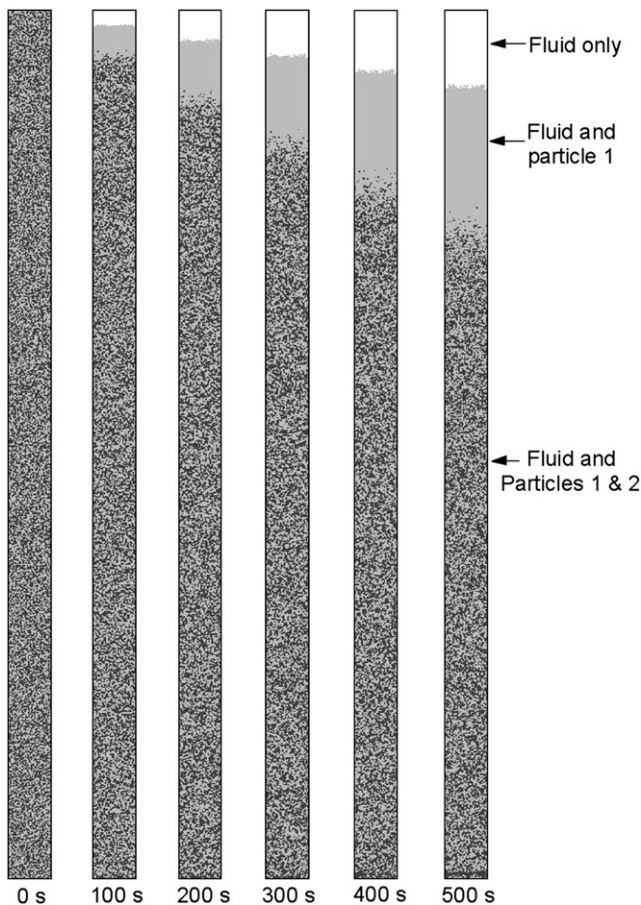
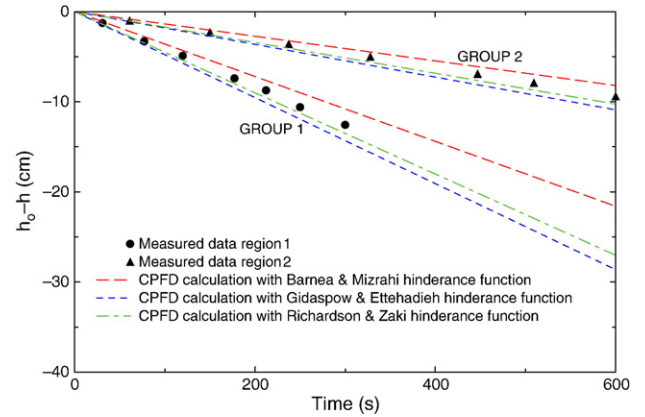function of particle volume fraction. Snider [5] developed the CPFD numerical scheme which includes features such as a subgrid particle stress model, particle forces such as particle friction, the tightly coupled solution of fluid and particle momentum and energy equations, and fast accurate solution methods for three dimensions. The body of this work is included in the Arena-flow® and Barracuda™ commercial software.

Three experiments which illustrate granular flow behavior are presented. The flows are particle sedimentation, flow from a hopper, and particles flowing into a U-tube. The CPFD method is applied to the three cases. All calculations are run in three dimensions and use the proper particle densities and particle size distribution (PSD).

2. CPFD governing equations

The CPFD method solves the fluid and particle momentum equations in three dimensions The fluid is described by the Navier–Stokes equation with strong coupling to the discrete particles. The particle momentum equations are ordinary differential equations with coupling to the fluid. The CPFD solution as applied in Arena-flow® and Barracuda-CPFD™ is aimed at solving commercial problems, which are generally physically large systems. In the CPFD scheme, a numerical-particle is defined where particles are grouped with the same properties (species, size, density, etc.). The numerical-particle is a numerical approximation similar to the numerical control volume where a spatial region has a single property for the fluid. Using numerical particles, large commercial systems containing billions of particles can be analyzed using millions of numerical-particles.

Fig. 2. CPFD calculated particle sedimentation.

Table 1
Hindrance functions multiplied times Stokes equation

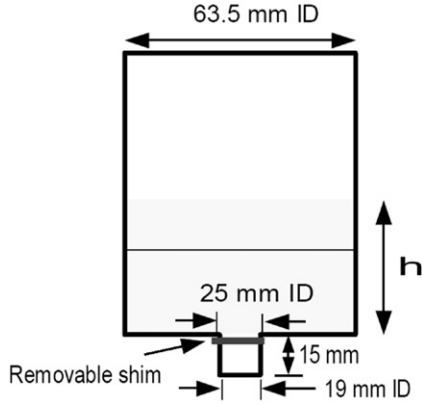| Gidaspow and Ettehadieh [12]	$C_d = \theta_f^{-2.65}$
Richardson and Zaki [13]	$C_d = \theta_f^{-4}$
Barnea and Mizrahi [14]	$C_d = \dfrac{(1 + \theta_p^{1/3})}{\theta_f^2} \exp\left(\dfrac{5\theta_p}{3\theta_f}\right)$

Fig. 4. Experimental hopper.

The volume average two-phase incompressible continuity equation for the fluid with no interphase mass transfer is

$$\frac{\partial \theta_f}{\partial t} + \nabla \cdot (\theta_f \boldsymbol{u}_f) = 0, \tag{1}$$

where $\boldsymbol{u}_f$ is the fluid velocity and θ_f is the fluid volume fraction. The volume average two-phase incompressible momentum equation for the fluid is

$$\frac{\partial (\theta_f \boldsymbol{u}_f)}{\partial t} + \nabla \cdot (\theta_f \boldsymbol{u}_f \boldsymbol{u}_f) = \frac{-1}{\rho_f} \nabla p - \frac{1}{\rho_f} \boldsymbol{F} + \theta_f \boldsymbol{g} + \frac{1}{\rho_f} \nabla \cdot \tau, \tag{2}$$

where ρ_f is fluid density, p is fluid pressure, τ is the macroscopic fluid stress tensor, and $\boldsymbol{g}$ is the gravitational acceleration. $\boldsymbol{F}$ is the rate of momentum exchange per volume between the fluid and particles phases. The fluid phase is compressible or incompressible (incompressible equations shown), and fluid and particle phases are isothermal.

The particle acceleration is

$$\frac{du}{dt} = D_p(\boldsymbol{u}_f - \boldsymbol{u}_p) - \frac{1}{\rho_p} \nabla p + \boldsymbol{g} - \frac{1}{\theta_p \rho_p} \nabla \tau_p + \boldsymbol{F}_S \tag{3}$$

where $\boldsymbol{u}_p$ is the particle velocity, ρ_p is the particle density, $\boldsymbol{g}$ is gravity and τ_p is the particle normal stress. The terms represent acceleration due to aerodynamic drag, pressure gradient, gravity and gradient in the interparticle normal stress, τ_p. The particle friction, $\boldsymbol{F}_S$ is opposite and limited to the relative particle motion, and only becomes important at very low particle flow at near close pack.

Particle properties are mapped to and from the Eulerian grid. The interpolation operator is the product of interpolation operators in the three orthogonal directions. For a particle located at $\boldsymbol{x}_p$, where $\boldsymbol{x}_p = (x_p, y_p, z_p)$, the x-directional component of the interpolation operator to grid cell i, is an even function, independent of the y and z coordinates, and has the properties.

$$S_i^x(\boldsymbol{x}_p) = \begin{matrix} 0 & x_{i-1} \geq \boldsymbol{x}_p \geq x_{i+1} \\ 1 & \boldsymbol{x}_p = x_i \end{matrix} \tag{4}$$

The x and y interpolation operators have a similar form. The particle volume fraction at cell ξ from mapping particle volume to the grid is

$$\theta_{p\xi} = \frac{1}{\Omega_\xi} \sum_l^{Np} \Omega_p n_p S_{p\xi} \tag{5}$$

where Ω_ξ is a grid volume, Ω_p is particle volume, n_p is the number of particles in a numerical particle, and the summation is over all numerical particles, N_p. From conservation of volume, the sum of fluid and particle volume fractions equals unity, $\theta_p + \theta_f = 1$.

The implicit numerical integration of the particle velocity equation is

$$u_p^{n+1} = \frac{u_p^n + \Delta t \left[D_p u_{f,p}^{n+1} - \frac{1}{\rho_p} \nabla p_p^{n+1} - \frac{1}{\rho_p \theta_p} \nabla \tau_p^{n+1} + \boldsymbol{g} + \boldsymbol{F}_S \right]}{1 + \Delta t D_p} \tag{6}$$

where $u_{f,p}^{n+1}$ is the interpolated fluid velocity at the particle location, $\nabla \tau_p^{n+1}$ is the interpolated pressure gradient at the particle location, ∇p_p^{n+1} is the interpolated particle stress gradient at the particle location, D_p is the drag coefficient. Particles are grouped into numerical-particles each containing n_p particles with identical properties located at position, $\boldsymbol{x}_p$. The new-time particle location is

$$x_p^{n+1} = x_p^n + \Delta t u_p^{n+1}. \tag{7}$$

The interphase drag coefficient is

$$D_p = C_d \frac{3}{8} \frac{\rho_g}{\rho_p} \frac{|\boldsymbol{u}_f - \boldsymbol{u}_p|}{r}, \tag{8}$$

where

$$\begin{aligned} \text{Re} < 1000 \quad & C_d = \frac{24}{\text{Re}} (1 + 0.15 \text{Re}^{0.687}) \theta_f^{-2.65} \\ \text{Re} \geq 1000 \quad & C_d = 0.44 \theta_f^{-2.65} \end{aligned} \tag{9}$$

The Reynolds number is defined as

$$\text{Re} = \frac{2\rho_f |u_f - u_p| r}{\mu_f}, \tag{10}$$

where μ_f is the gas viscosity and the particle radius is

$$r = \left(\frac{3\Omega_p}{4\pi} \right)^{1/3} \tag{11}$$

To check the sensitivity of drag on sedimentation, the sedimentation calculations were run with three different drag models.

Particle-to-particle collisions are modeled by a particle normal stress. The particle stress is derived from the particle volume fraction which, in turn, is calculated from particle
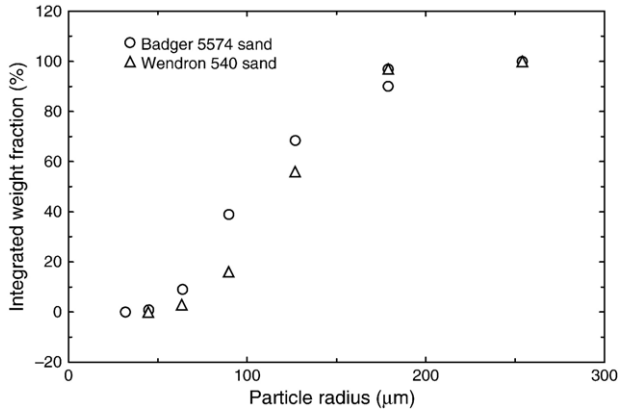
Fig. 5. Particle size distribution. The granular material is sand with density 2760 kg/m³.

volume mapped to the grid. The particle normal stress model used here is

$$\tau = \frac{P_s \theta_p^\beta}{\max[(\theta_{CP}-\theta_p), \varepsilon(1-\theta_p)]}, \qquad (12)$$

where ε is a small number on the order of 10^{-7} to remove the singularity. The close-pack limit is somewhat arbitrary and depends on the size, shape and ordering of the particles. Therefore the solution method allows the particle volume fraction, at times, to slightly exceed close pack which is physically possible considering that shifting or rearranging of granular materials may occur. The particle normal stress is mapped and applied to discrete particles. Because particles have subgrid (no grid) behavior, the application of the normal stress gradient to a discrete particle is modeled and accounts for the particle properties and whether the particle is moving with or against the stress gradient.

A characteristic of granular flow is that particles stack to form a pile with an "angle of repose" describing the pile's slope. The particle normal stress model inherently gives an angle of repose. Fig. 1 illustrates particles at the surface of a packed bed. The movement into the bed is stopped by the vertical component of the particle normal stress, but the particle is moved sideways by the horizontal component of the particle normal stress. If particles come to rest, the horizontal component of the particle stress gradient continually forces particles sideways with a diminishing force as the angle of repose decreases. Without a stabilizing surface force, such as static friction or surface tension, the particle normal force, over a long time, will eventually collapse the granular pile.

Static friction from first principles can only be done for the most simple case, and methods, such as DEM use a static friction model to capture the particle interface physics. The complexity increases by orders of magnitude when the surfaces are not planes such as contact between irregular solids. The complexity and computational-work further increases for three-dimensional DEM modeling. Average static and dynamic contact friction is modeled well as a friction force proportional to the solid normal force, F_N,

$$\boldsymbol{F}_S = c_s F_N \qquad (13)$$

The proportionality constants, c_s, is the experimentally determined coefficient of friction. Within a static particle bed where gravity and enduring contact (particle pressure) are the dominant forces, a static frictional force model [18] has a straight forward implementation to each particle. The normal force of solid-on-solid is calculated from the local particle normal particle stress with the partial redirection of force from mini-arching between solids being modeled by a Janssen coefficient [15]. A numerical benefit of the static friction within the bed is to damp small, high frequency solids motion (jitters)
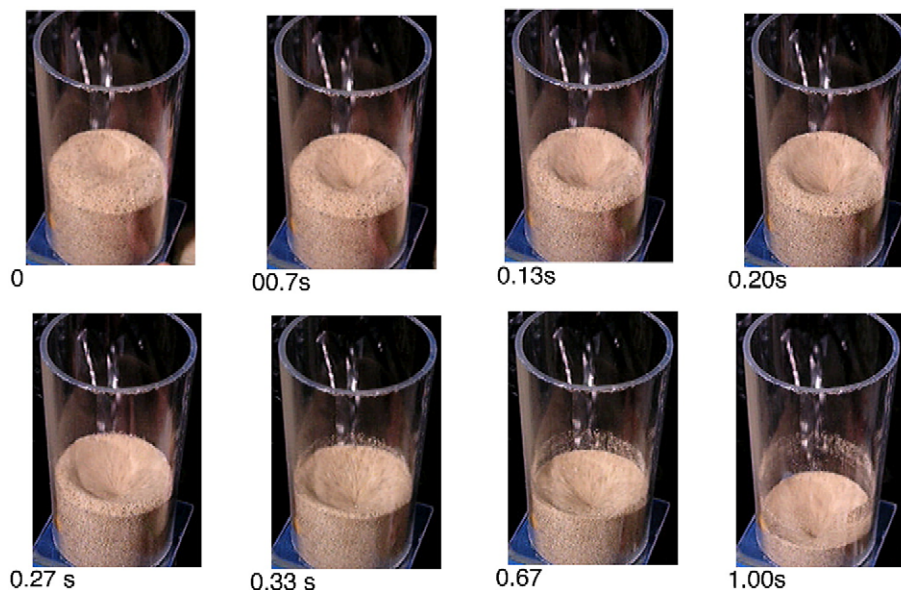

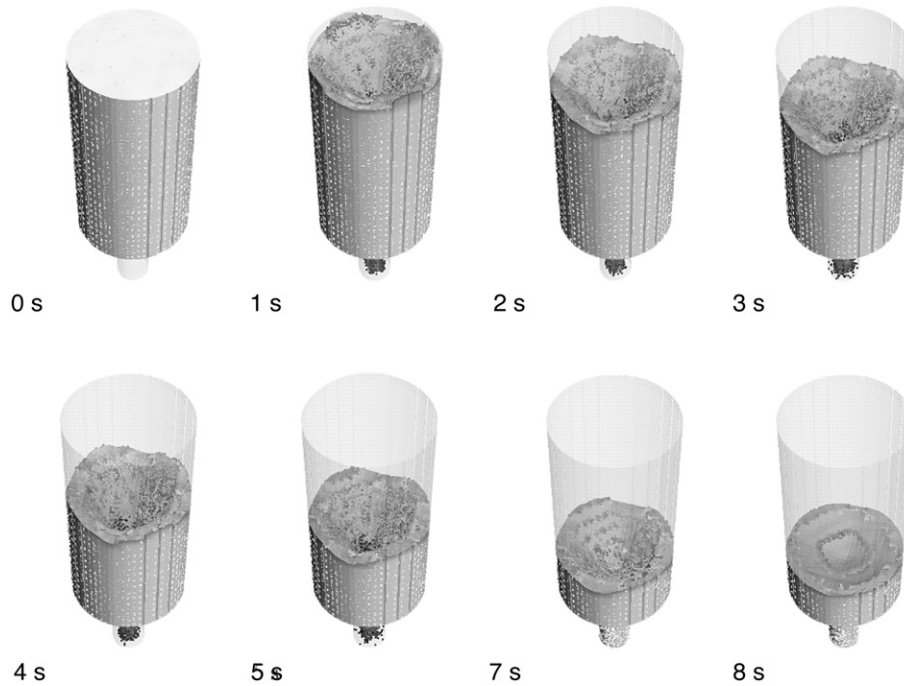Fig. 6. Emptying from hopper tank.

Fig. 7. Calculated particle field during hopper tank emptying.

produced by the very large, non-linear particle pressure gradient at close pack.

The static friction is more difficult to implement on a complex three-dimensional surface of solids. The dominant force may not be gravity which conveniently has a constant direction, but the normal force to a packed region of solids may depend on motion of the solids. The same basic model, used within a static packed bed, is applied to the more complex free surface and directionally non-constant normal-forces. A particle on an inclined surface can slip or roll and possibly bounce down the surface. Particles can also form bridges or can wedge into crevices which retard motion, and bonds can form between particles such as those from surface tension which restrict particle flow. While the mechanisms for rolling, slipping and bouncing of particles along the incline are different; the process

is modeled as an average friction force which is proportional to the particle normal force, Eq. (13).

In applying the CPFD method, a granular-material slope is estimated in the direction of the particle motion. The slope is determined from the particle volume fraction in a plane of cells where the particle resides and the particle volume fraction in the next grid—plane up or down depending on whether the particle force is positive or negative, respectively. The friction force is the friction-coefficient times the normal component of the
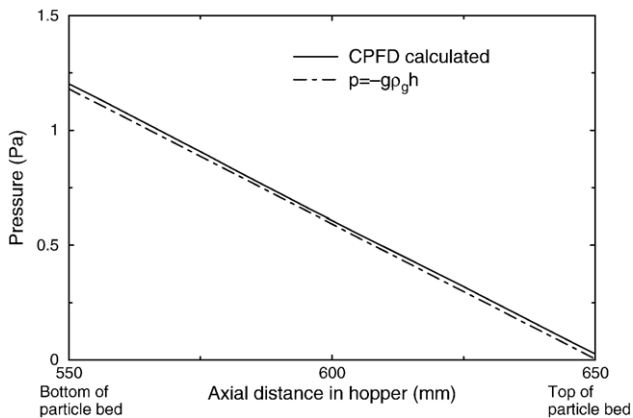

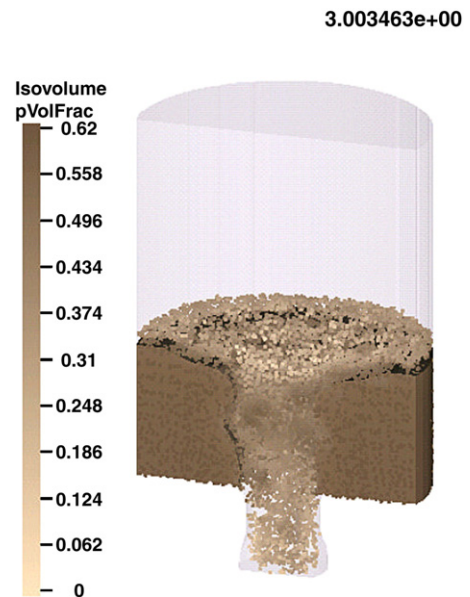Fig. 8. Static pressure in the hopper prior to emptying.

Fig. 9. Calculated particle flow where particles are colored by local volume fraction.
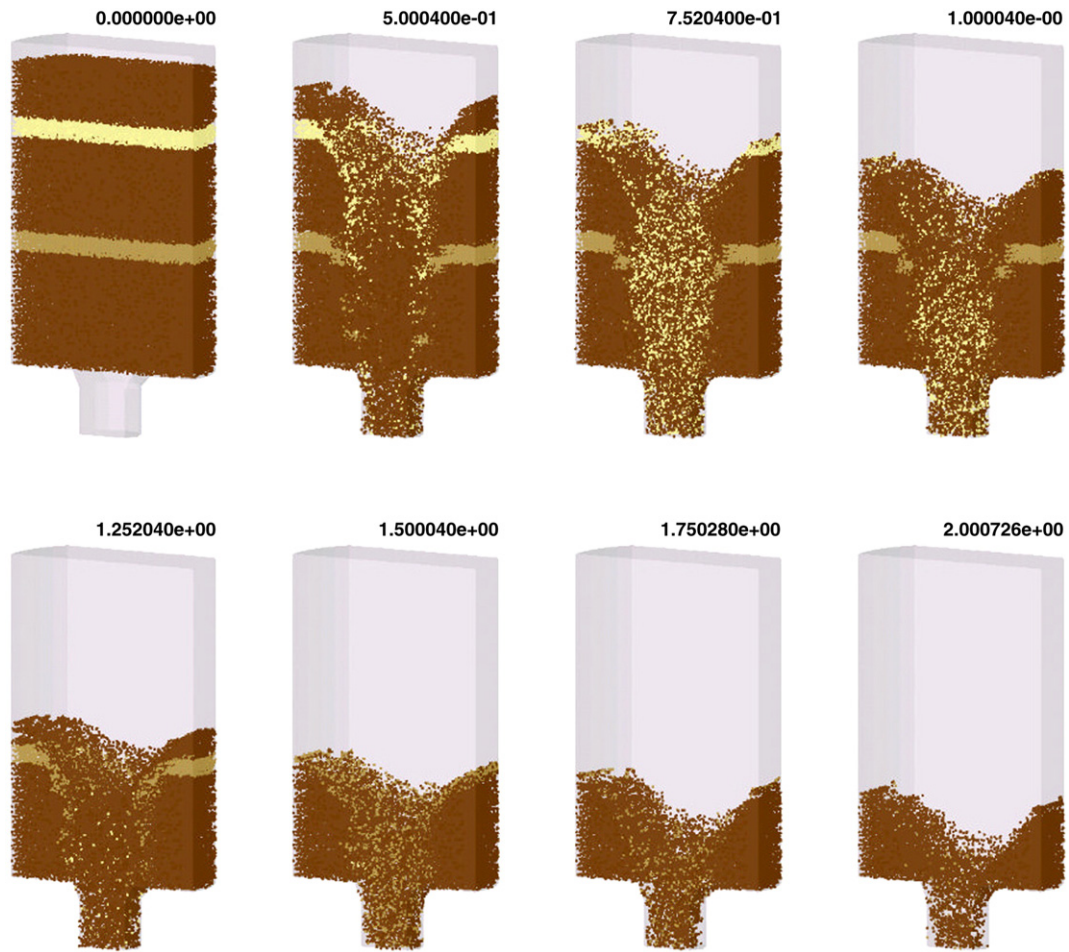
0.000000e+00   5.000400e-01   7.520400e-01   1.000040e-00

1.252040e+00   1.500040e+00   1.750280e+00   2.000726e+00

Fig. 10. Two layers of colored particles in the hopper. The view is a center slice through the vessel.

particle's forces relative to the material slope. The friction force exponentially decays with decreasing volume fraction and exponentially decays with increasing relative particle velocity which provides for the difference between static and dynamic friction. For flowing particles or particles not near close pack, the static friction force goes to zero.

The conservation equations are approximated and solved by finite volumes with staggered scalar and momentum nodes. The fluid momentum equation implicitly couples fluids and particles through the interphase momentum transfer. The interphase momentum transfer at momentum cell ξ is

$$F_\xi^{n+1} = \frac{1}{\Omega_\xi} \sum_p S_\xi \left[D_p(u_{f,p}^{n+1} - u_p^{n+1}) - \frac{1}{\rho_p} \nabla p_p^{n+1} \right] n_p m_p, \qquad (14)$$

Particle drag and properties are interpolated to the grid. If a top hat interpolation is used, the fluid velocity at particle position x_p is either zero or the node velocity. If a bilinear or other interpolation is used, the fluid velocity at particle position x_p includes the node velocities in support of the interpolation.

The drag force is particle dependent, i.e. depends on particle size, shape and possibly other geometrical properties. Further, each particle sees a unique fluid property (viscosity, velocity, etc) at a particle location from an interpolation from 8 Eulerian

cells in support of the interpolation operator. This is also true of the fluid phase in that the local drag of each particle is included in the fluid equation (millions of numerical particles). The drag force on fluid in an Eulerian control volume is from interpolation of drag force from particles in 27 Eulerian control volumes in support of the interpolation operator. The inclusion of particle momentum also includes the local pressure gradient at particle locations. Further the particle momentum is an
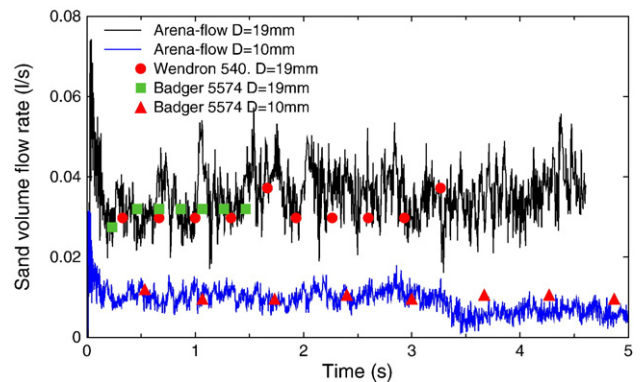

Fig. 11. Comparison of measured and calculated particle flow rate from hopper.
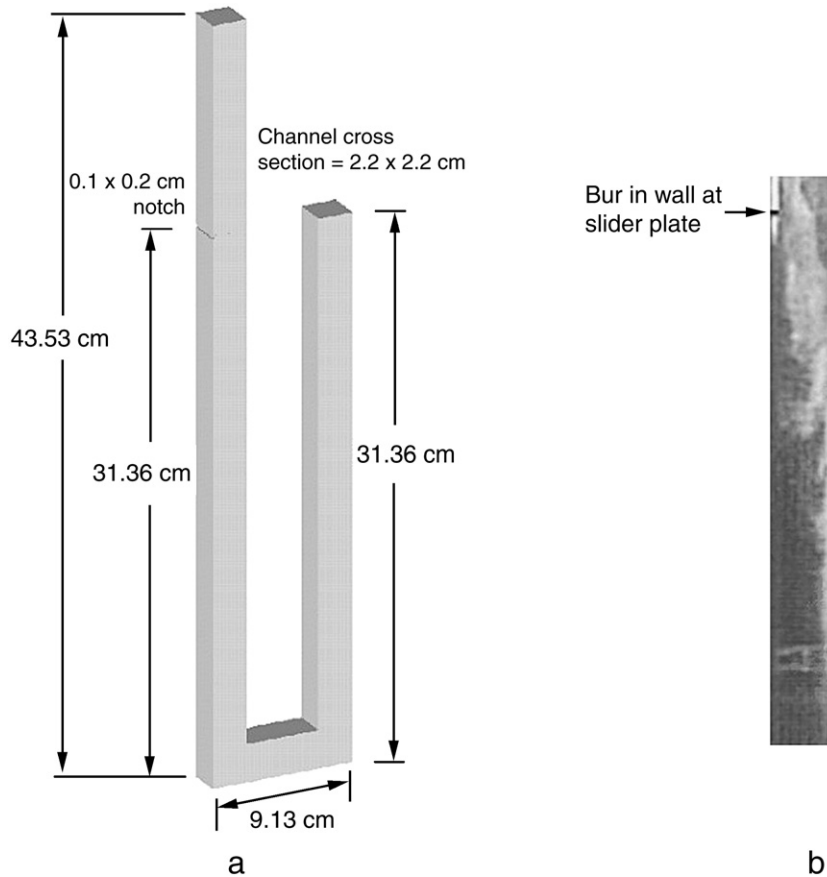
Fig. 12. U-tube experiment dimension and particle flow at the slider shim.

implicit coupling in the fluid phase which provides a robust solution, especially for small particles which produce very high drag. The coupling of fluid and particles gives a subgrid influence in the Eulerian solution. One easy thought on the subgrid behavior is the motion of a large and small particle within an Eulerian control volume. The larger particle may be dominated by the body force and move down while the small particle next to the large particle may be dominated by the

aerodynamic drag and move upward. This subgrid particle motion is coupled into the fluid phase.

Mass continuity is from the material motion of particles. The fluid mass is calculated from volume continuity, $\theta_f = 1 - \theta_p$. A SIMPLE solution scheme is used to adjust pressure and fluid velocity to satisfy fluid continuity. Velocity and pressure correction dependence, estimated from the momentum equation are entered into the fluid continuity equation, giving a semi-
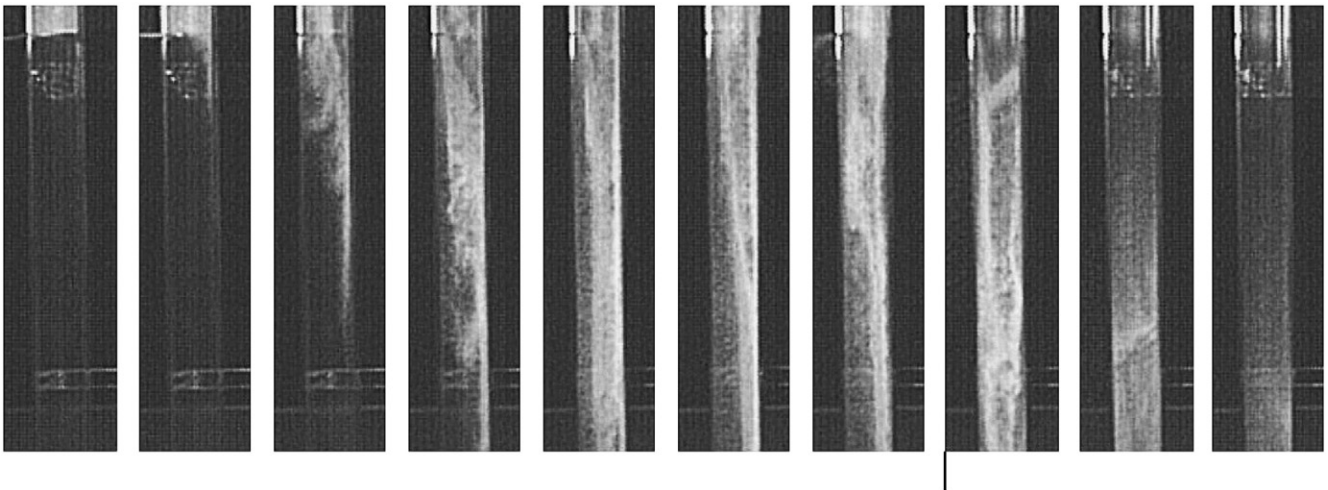

Fig. 13. Solids flow in the vertical arm of the U-tube experiment.

Fig. 14. CPFD calculated U-tube filling.

implicit coupling of mass and momentum in a pressure correction equation. The pressure equation is solved and fluid pressure and velocities are corrected to satisfy continuity.

3. Sedimentation

Homogeneous, batch sedimentation begins with a uniform distribution of suspended particles in a container. If left alone, the particles separate from the fluid into distinct regions of particles that depend on the particle densities and sizes. A suspension with a variety of particle sizes and densities will form multiple regions, where each region above the previous region contains one less species, where a species is a group of particles with near the same particle size and density. The top of

the vessel will be clear fluid (providing particle densities are greater than the fluid density) and the bottom of the vessel will contain all species. In cases where there is a large variation between sizes and/or density of species, the regions are distinct and separated by strong concentration gradients Davis and Acrivos [9] and Al-Naafa' and Selim [10] provide reviews of experiments and analysis of polydisperse suspensions.

The settling of one or a few particles size can be predicted by a Eulerian particle solution. The Eulerian solution becomes far more difficult with more than a few particle sizes or densities, because of the increased computation expense for solving many conservation equations. For a wide distribution of particle sizes, using an average particle size will not give a good prediction of the settling rate. The CPFD method has virtually unlimited size
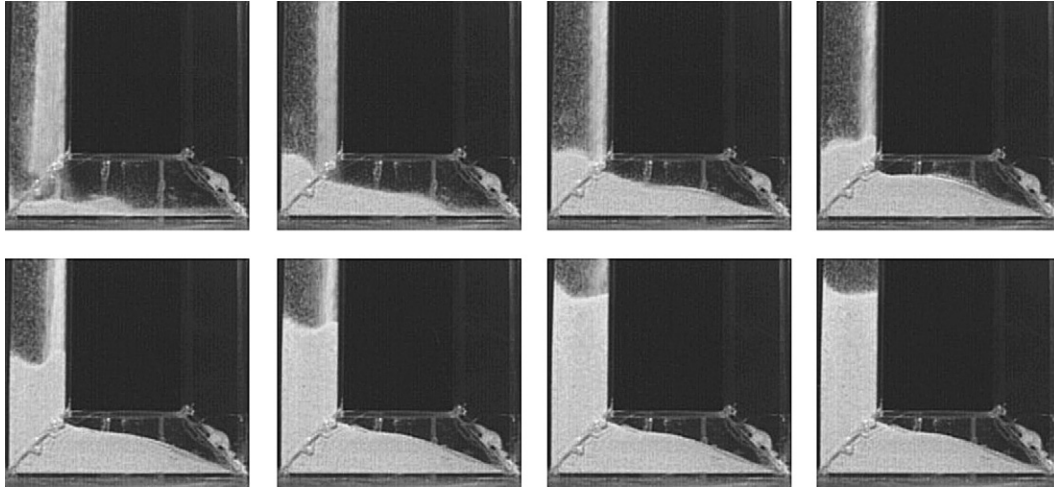
Fig. 15. Particle flow in the U-tube section.

and density of particles and can capture the settling physics well whether there are few or many particle sizes.

The bimodal suspension of a glass beads experiment given by Davis et al. [11] was calculated by Snider [8] and again in this study in three dimensions using the CPFD method. The vessel is vertical and the fluid density and viscosity are 992 kg/m³ and 0.0667 kg/(m-s), respectively. The small glass bead density is 2440 kg/m³, and beads range in diameter from 125 to 150 μm. The larger bead density is 2990 kg/m³ and beads range in diameter from 177 to 219 μm. The calculation uses a uniform random distribution within the reported experimental size ranges. Initial volume fractions for the small and large beads are 3% and 1%, respectively.

Fig. 2 shows the calculated particles which separate into three distinct sedimentation regions. There is an interplay of heavy, large particles and light, small particles. The heavier particles have a larger gravity force, and the smaller particles have a larger fluid drag. In the experiment (and calculation), the combination of small, light particles are in the first fluid–particle layer. The second particle layer contains both size and density particles. With different particle densities and sizes, there can be sedimentation with the heavier particles in the first particle layer, and heavy and lighter particles in the lower particle layer, depending on sizes and densities. In Fig. 2, the layers are distinct, but there is a sight blurring at interfaces. This slight smearing at the interface is because a normal distribution of particle size about the experiment size range is used. There are small particles with slightly higher drag that slightly separate from the bulk-particles at the second interface.

The predicted rate of sedimentation compared to measured data are shown in Fig. 3. As one might expect, the predicted sedimentation rate depends on the drag correlation. To gauge the influence of drag models, three calculations are shown using three drag hindrance models which are listed in Table 1. All three drag models gave a good comparison with measured data. The CPFD calculation was for a bimodal suspension experiment, but could have as easily been applied to suspension of many different size and density particles. Sedimentation of particles with narrow size and density ranges give distinct

layers. More important for commercial applications is the sedimentation of solids with a wide distribution in particle sizes and/or densities. The CPFD method would accurately calculate the particle settling of these commercial applications where a pseudo-continuum calculation using one or maybe two average particle size would not fare well.

4. Hopper flow

The complex flow in the seemingly simple hopper has been studied extensively over the years. Early work by Janssen [15] and others experimentally showed that a granular material exerts a lateral force on bin walls, but the force is far less than a fluid hydrostatic pressure force and eventually becomes bed-depth insensitive. Empirical or simple force balances models have been the primary method to predict the particle discharge in commercial hoppers. Jenike [16] used a steady-state force balance on particles and the hopper wall to model the hopper flow. Beverloo et al. [17] and Johanson [18] provide two simple models to predict hopper discharge rates. Many of the fluid solutions to particle flow are two-dimensional, and most DEM predictions of hopper flow have been two-dimensional where particles are modeled as rods or the fluid is neglected. With increased computation power and better algorithms, more three-dimensional DEM calculations are being presented [19,20].

The lab-scale hopper experiment is illustrated in Fig. 4. The hopper connects to a short discharge tube. The fluid is air, and the granular material is sand from two manufactures. The sand density is 2760 kg/m³, and the particle size distributions are shown in Fig. 5. The emptying of the hopper into a graduated cylinder is filmed, and knowing the frame rate and the level in the graduated cylinder, the flow rate from the hopper is calculated. The measured solid volume is both particles and air, and to get the solid flow rate, the measured volume is multiplied by the particle close-pack volume fraction of 0.64.

Fig. 6 shows time-frames of the hopper as it empties. A cone depression forms at the top, and the depression remains relatively constant during the emptying. The hopper experiment shown in Fig. 6 empties into a container which fills, and the
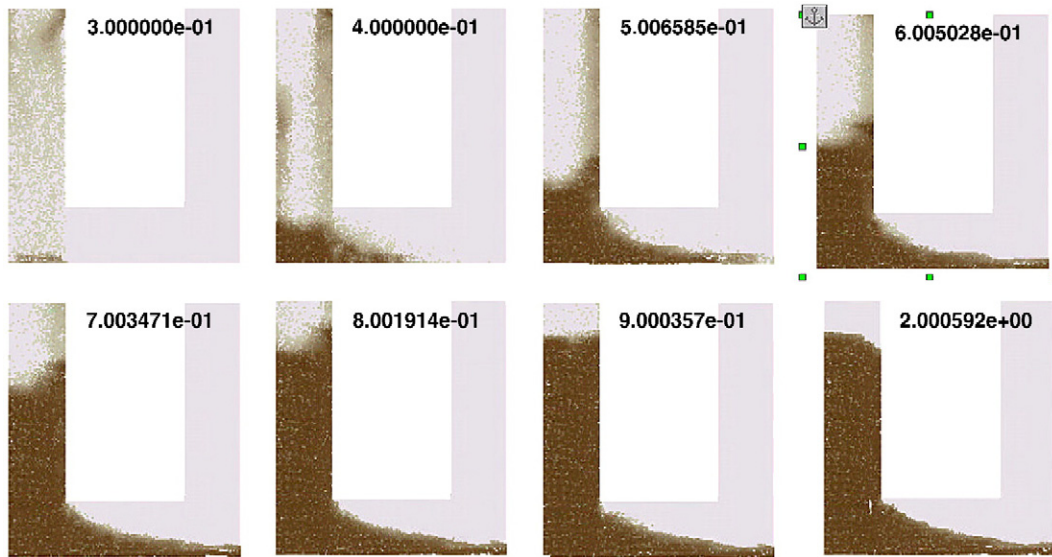
Fig. 16. Detail of CPFD calculated sand flow in a U-channel.

hopper does not completely empty. The majority of other tests completely empty the hopper. Fig. 7 shows the CPFD predicted emptying of the hopper with a backfill stopping the particle flow which matches the experiment. The agreement between calculated and measured appearance during emptying is good.

Particles are not forced out of the bottom of the hopper by a hydrostatic "head" of particles which would give the discharge rate dependent on bed height. A purely fluid model for sand without proper modeling of particle forces would incorrectly give a high hydrostatic pressure at the bottom of the tank. The CPFD calculated pressure in the tank, prior to opening the bottom hole, gives the correct pressure which is a hydrostatic column of air as shown in Fig. 8.

Fig. 9 shows particles during the emptying of the hopper with the front of the hopper cut-away. The particles are colored by local solids volume fraction. Dark-brown is close pack. Particles, emptying from the bottom, produces a low volume fraction region allowing particles above to flow into the void (driven by gravity). As time progresses, a kinematic volume fraction wave (dialation) moves up through the center of the hopper tank. Fig. 10 shows the hopper with two initial layers of colored particles at two levels in the hopper. During the hopper emptying, particles away from the center remain relatively stationary until the central bed-level drops, and allows particles across the bed to move into the central cone. Fig. 11 compares the CPFD predicted discharge rate with the measured rate. The predicted particle flow rate compares well with the measured flow rate, and the discharge rate is relatively constant as it should be.

5. Particles flow in a U-tube

A well known behavior of particles is that they stack with an "angle-of-repose". It is also difficult to fill a container with granular material when the container has an irregular shape or has a complex flow channels. A fluid, on the other hand will completely fill the most complex geometry container up to a hydrostatic level. The granular flow behavior is illustrated in a U-tube. The U-tube is shown in Fig. 12.

Sand is placed on top of a shim in the long vertical arm. The sand is Badger 5574 with a density of 2760 kg/m^3, and a particle size distribution given in Fig. 5. The shim is quickly removed and sand is filmed at 1000 frames per second as it falls into the U-section.

Fig. 12 shows the initial particle flow in the upper section under the shim slot. The rectangular tube has a burr at the cut for the shim slot, and the initial removal of the shim and the burr produced a non-uniform particle flow pattern. The burr was not intended to be part of the experiment, but because it was there, it was included in the CPFD calculation. In general, the falling of dense material through a light fluid will give instabilities similar to Rayleigh–Taylor flow. Fig. 13 shows the measured transient flow of solids in the vertical arm, and Fig. 14 shows the CPFD calculated flow of sand in the U-tube. The calculation also includes the burr at the slider slot which produces similar flow patterns as observed in the experiment. Both the appearance and rate of solid flow compares well to the experiment.

Fig. 15 shows measured sand flowing into the bottom of the U-tube. The last frame in Fig. 15 is the final, static sand distribution which is a partial fill of the U-bend. Fig. 16 shows the CPFD calculated filling in the U-bend which compares well with the measured data. If particles are modeled as a fluid, the fluid would fill both arms to a constant level (manometer), predicting an incorrect behavior for particle flows. The ability to predict this phenomenon is essential to many industrial applications, for example the filling of sand-cores widely employed in metal castings.

6. Concluding remarks

Three experimental examples of easy-to-comprehend granular flow are presented which are not modeled or not modeled

well by a pseudo-continuum approximation for particle flow. The flows are predicted with a computational particle fluid dynamic (CPFD) numerical scheme, in three dimensions using the correct PSD. The CPFD calculations gave excellent prediction of all three experiments. The calculations use the same numerical scheme for all cases with no adjustment in the method or models to account for a special characteristic of the particle flow.

The accurate prediction of the particle flow in this study is important for two reasons. First it illustrates and verifies the CPFD calculation ability for predicting particle flow. Second, any numerical scheme needs to be tested on fundamental problems with known behavior before it can be applied to large commercial problems. By predicting fundamental physics of granular flow, confidence is gained that the numerical tool accurately predicts large complex systems where there is little or no measured data.

References

[1] G.K. Batchelor, A new theory of the instability of a uniform fluidized bed, J. Fluid Mech. 193 (1988) 75–110.

[2] D. Gidaspow, Hydrodynamics of fluidization and heat transfer supercomputer modeling, Appl. Mech. Rev. 39 (1986) 1–22.

[3] M.A. Risk, Mathematical modeling of densely loaded, particle laden turbulent flows, At. Sprays 3 (1993) 1–27.

[4] P.J. O'Rourke, Collective drop effects on vaporizing liquid sprays, PhD. Thesis, Princeton University (1981).

[5] D.M. Snider, An incompressible three dimensional multiphase particle-in-cell model for dense particle flows, J. Comput. Phys. 170 (2001) 523–549.

[6] P.J. O'Rourke, A.A. Amsden, On particle-grid interpolation and calculating chemistry in particle-in-cell methods, J. Comput. Phys. 109 (1983) 37–52.

[7] M.J. Andrews, P.J. O'Rourke, The multiphase particle-in-cell (MP-PIC) method for dense particle flow, Int. J. Multiph. Flow 22 (1996) 379–402.

[8] D.M. Snider, P.J. O'Rourke, M.J. Andrews, Sediment flow in inclined vessels calculated using multiphase particle-in-cell model for dense particle flow, Int. J. Multiph. Flow 24 (1998) 1359–1282.

[9] R.H. Davis, A. Acrivos, Sedimentation of noncolloidal particles at low Reynolds numbers, Annu. Rev. Fluid Mech. 17 (1985) 91–118.

[10] M.A. Al-Naafa', M.S. Selim, Sedimentation of polydisperse concentrated suspensions, Can. J. Chem. Eng. 67 (1989) 253–263.

[11] E. Davis, R.H. Herbolzheimer, A. Acrivos, The sedimentation of polydisperse suspensions in vessels having inclined walls, Int. J. Multiph. Flow 8 (6) (1982) 571–585.

[12] D. Gidaspow, B. Ettehadieh, Fluidization in two-dimensional beds with a jet, Part II: hydrodynamic modeling, I&EC Fundam. 22 (1983) 193–201.

[13] J.F. Richardson, W.N. Zaki, Sedimentation an fluidization: Part I, Trans. Inst. Chem. Eng. 32 (1954) 35–53.

[14] E. Barnea, J. Mizrahi, A generalized approach to the fluid dynamics of particle systems: Part 1. General correlation for fluidization and sedimentation in solid multiparticle systems, Chem. Eng. J. 5 (1973) 171–189.

[15] H.A. Janssen, Tests on grain pressure silos, Z. Ver. Dtsch. Ing. 39 (35) (1895) 1045–1049.

[16] A.W. Jenike, Storage and flows of solids, Bulletin No. 123 of the Utah Engineering Experimental Station, vol. 53, University of Utah, 1964, p. 26.

[17] W.A. Beverloo, H.A. Leniger, J. von der Velde, The flow of granular flow through orifices, Chem. Eng. Sci. 15 (1961) 260.

[18] J.R. Johanson, Stress and velocity fields in the gravity flow of bulk solids, J. Appl. Mech., E 86 (1964) 499.

[19] T.J. Goda, F. Ebert, Three-dimensional discrete element simulation in hoppers and silos, Powder Technol. 158 (2005) 58.

[20] P.W. Clearly, M.L. Sawley, DEM modeling of industrial granular flows: 3D case studies and the effect of particle shape on hopper discharge, Appl. Math. Model. 26 (2002) 89.